RSC Advances




ROYAL SOCIETY OF CHEMISTRY

www.rsc.org/advances

Journal Name

RSCPublishing

ARTICLE

# Flower-like $In_2O_3$ hierarchical nanostructures: synthesis, characterization, and gas sensing properties

Cite this: DOI: 10.1039/xoxxoooooox

Received ooth January 2012,
Accepted ooth January 2012

DOI: 10.1039/xoxxoooooox

www.rsc.org/

Dan Han, Peng Song *, Huihui Zhang, Huihui Yan, Qi Xu, Zhongxi Yang, Qi Wang *

Hierarchical $In_2O_3$ nanostructures with flower-like morphology were synthesized by annealing $In(OH)_3$ precursor prepared via a one-step hydrothermal method using the mixed solution of N, N-dimethylformamide (DMF) and deionized water as solvent. The crystal structure and morphology of the obtained samples were characterized by X-ray diffraction (XRD), scanning electron microscope (SEM), transmission electron microscope (TEM), and $N_2$ adsorption-desorption analyses. The results revealed that the synthesized flower-like $In_2O_3$ hierarchical nanostructures were constructed from $In_2O_3$ nanoplates which connected with each other to form flower-like architecture. On the basis of experimental results, a possible mechanism for the formation of flower-like $In_2O_3$ hierarchical nanostructures was speculated. Moreover, gas sensing investigation showed that the sensor based on flower-like $In_2O_3$ hierarchical nanostructures exhibited superior response, good selectivity and stability to ethanol gas. The enhancement in gas sensing properties was attributed to their unique structure, large surface areas, and more surface active sites.

## Introduction

Ethanol sensing has been widely applied in various fields, such as in ethanol breath analyzers for detecting ethanol vapor in the drivers' breath, in foodstuffs experiments to assess the development of bacteria and fungi in food, in monitoring the biomedical and chemical processes in chemical industries and so on.[1-3] Thus, growing concern about air pollution with respect to public health has enhanced the demand for gas sensors for monitoring ethanol concentration in the environment. Metal oxide semiconductor gas sensors have attracted much attention for their diverse applications in ethanol detection. Until now, a number of ethanol-sensing sensors based on $SnO_2$,[4] ZnO,[5] $LaFeO_3$,[6] and $WO_3$[7] have been successfully obtained. As an important n-type semiconductor, indium oxide ($In_2O_3$) with high chemical and thermal stability has attracted considerable research efforts in its applicability as gas sensors.[8-11] Recently, $In_2O_3$-based sensors have been investigated for the detection of ethanol vapor at various concentration levels.[12-15]

As we known, the crystal phase, morphologies, as well as the porosity have a profound influence on the sensing performance of $In_2O_3$ nanomaterials. Therefore, the design and tailor of $In_2O_3$ nanomaterials with different morphologies and structures are very important in view of both basic fundamental research and the development of novel devices. To meet the demand for practical applications, various $In_2O_3$ nanostructures have been fabricated, including nanoparticles,[16] nanowires and nanorods,[17] nanoplates or nanosheets,[18] and 3D hierarchitectures.[19-20] Being a special kind of nanostructure, 3D hierarchical nanostructures have become strategic for various applications mainly due to their large specific surface area and desirable surface permeability. Actually, these favorable properties are also significant for gas sensing, which can allow fast diffusion for target gases to interact with the entire sensing layer. To date, much effort has been given to prepare the 3D hierarchical $In_2O_3$ structures by many synthetic strategies. For these approaches, the hydrothermal synthesis method has been proved to an effective technique, which has the obvious advantages of simple, mild, and high yields.[21, 22] In our previous work, 3D porous $In_2O_3$ nanospheres consisted of numerous tiny $In_2O_3$ nanoparticles were synthesized by hydrothermal synthesis method, which exhibited higher response to ethanol gas compared with that of commercial bulk $In_2O_3$ particles.[23] Hence, it is strongly desirable for the fabrication of the porous $In_2O_3$ hierarchical nanostructures by exploring more simple and effective techniques. However, despite this recent progress, there are still some difficulties in the organization of 2D building blocks (e.g. nanosheets or nanoplates) into 3D superstructures, especially when they need to be porous and thus possess a high surface area.

It is also noted that additive-free synthesis of nanostructures and self-assembling them into well-defined structures remains a huge challenge. Herein we report a successful facile self-assembly, template and additive-free synthesis route toward achieving flower-like $In_2O_3$ hierarchical nanostructures consisted of $In_2O_3$ nanoplates via an oriented attachment growth mechanism. The synthesis entails preparation of the intermediate $In(OH)_3$ precursors under hydrothermal conditions using $InCl_3$ as a precursor, a mixed solvent

system of water and N, N-dimethylformamide (water/DMF) as the reaction medium. The products were characterized by FESEM, TEM, and nitrogen sorption. According to the experimental results, a possible formation mechanism was proposed and its ethanol sensing properties were investigated.

## Experimental

### Synthesis of flower-like $In_2O_3$ hierarchical nanostructures

In the experiments, all the chemical regents were analytical grade and used without further purification. In a typical experiment, 0.5 mmol $InCl_3 \cdot 4H_2O$ was first dissolved in the mixed solution of 15 mL distilled water and 15 mL DMF at room temperature, followed by addition of 1 mmol $Na_3C_6H_5O_7 \cdot 2H_2O$ under vigorous stirring. Subsequently, 2 mmol of urea was added into the above mixed solution under vigorous stirring. The reaction mixture was transferred into a Teflon-lined stainless-steel autoclave and kept at 170 $^oC$ for 14 h. After the hydrothermal procedure, the autoclave cooled naturally down to room temperature. The precipitates were collected by centrifugation, washed several times with deionized water and ethanol, respectively, and dried at 60 $^oC$ for 12 h. Finally, flower-like $In_2O_3$ hierarchical nanostructures were obtained by annealing the precipitates at 500 $^oC$ for 3 h in air atmosphere.

### Characterization

The crystal structure and phase composition of samples were identified by the means of X-ray diffraction (XRD, Bruker D8 Advance) using Cu*Ka*1 radiation ($\lambda$ = 0.15406 nm) at 30 kV and 40 mA at a scanning rate of 2$^o$ at 2$\theta$ min$^{-1}$ ranging from 20$^o$ to 80$^o$, and energy dispersive X-ray spectroscopy, the morphology and the microstructure of the products were characterized by field emission gun scanning electron microscope (FESEM, Hitachi S4800), transmission electron microscopy (TEM, Hitachi H-800) and high resolution electron microscopy (HRTEM, JEOL 2010). The specific surface area was estimated using the Brunauer–Emmett–Teller (BET) method based on the $N_2$ adsorption-desorption tests. Pore-size distribution was calculated from the adsorption branch of the nitrogen isotherm, using the Barrett–Joyner–Halenda method applied to the desorption part of the adsorption-desorption isotherm.

### Gas sensor fabrication and response tests

The fabrication progress of the gas sensor was as follows: the as-obtained final product was ground and mixed with deionized water in order to form paste in agate mortar, which was evenly smeared onto the outer surface of a ceramic tube by hair brush to form a thick film to cover a pair of Au electrode, which had been printed on the tube previously. Four Pt lead wires attaching to the Au electrodes were used for measurement and a Ni-Cr alloy coil through the tube as a heater to operating the temperature. After dried in the air and aged at aging set at 2 days, it has been an indirectly-heated gas sensor, and then the gas sensor was put into the test chamber in a measuring system of WS-30A (Winsen Electronics Co. Ltd., Zhengzhou, China) by a static process.[24, 25] Then, the sensors were put into a glass chamber at the beginning. When the resistances of all the sensors were stable, the calculated amount of the target gas or liquid was injected into glass chamber by a micro-injector and mixed with air. After the sensor resistances reached a new constant value, the test chamber was opened to recover the sensors in air. All the measurements were performed in a laboratory fume hood with a large draught capacity. The sensor resistance and response values were acquired by the analysis system automatically. The whole experiment process was performed in a super-clean room with the constant humidity and temperature. In the test process, a working voltage of 5 V ($V_{working}$) was applied. By monitoring the voltage across the reference resistor ($V_{output}$), the response of the sensor in air or in a test gas could be measured. The sensor response was defined as,

$$Response = R_{air}/R_{gas} \quad (1)$$

where $R_{air}$ is the resistance of the sensor in air and $R_{gas}$ is the resistance of sensor in the presence of the test gas. Then, the slope coefficient of response value to the logarithm of the concentration was defined as sensitivity. The response and recovery time was defined as the time taken by the sensors to achieve 90% of the total resistance change in the case of adsorption and desorption, respectively.

## Results and discussion

### Crystal structure and morphology

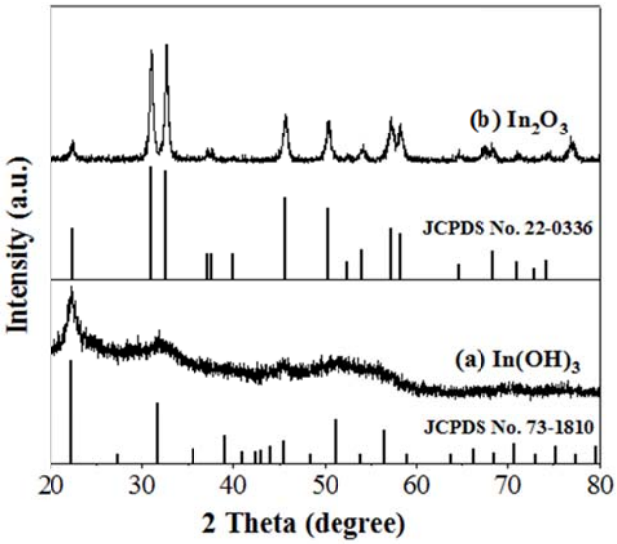


Fig. 1 XRD patterns of the $In(OH)_3$ precursors and as-synthesized $In_2O_3$ products.

The crystal structure of the prepared samples was characterized by X-ray diffractometer. As shown in Fig. 1, the diffraction peaks of the precursor (curve a) are in good agreement with cubic structure $In(OH)_3$ (JCPDS No. 73-1810), no peaks for other impurities are detected. After annealing at 500 $^oC$, all the peaks of the sample (curve b) are indexed to the hexagonal phase of $In_2O_3$ with the standard date file (JCPDS file No. 22-0336). No other phases were observed, confirming the precursor has completely transformed into the pure hexagonal $In_2O_3$ crystal. Compared with those of the bulk material, the peaks were relatively broadened, which demonstrated that the $In_2O_3$ had a small crystal size. Further, the crystallite size is estimated using the Scherrer formula:

$$D = 0.89\lambda/\beta\cos\theta \quad (2)$$

where $D$ is the mean crystallite size, $\lambda$ is the wavelength of the X-ray radiation ($\lambda$ = 0.154 nm for Cu*Ka*1 radiation), and $\beta$ is the full width

at half-maximum of diffraction peak at 2$\theta$. The average crystallite size of the as-prepared $In_2O_3$ sample was approximately 18.2 nm.

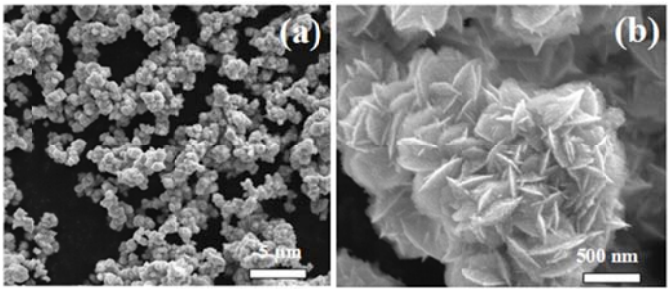


Fig. 2 (a) Low and (b) high magnification FESEM images of the as- prepared $In(OH)_3$ precursors.

The morphology of as-prepared $In(OH)_3$ precursor was demonstrated by FESEM, as shown in Fig. 2. It can be seen that the sample was composed of a large number of flower-like architecture with diameters of about 1.5-2 μm (Fig. 2(a)). Furthermore, the 3D flower-like architecture was consisted of many 2D nanoplates of $In(OH)_3$ (Fig. 2(b)). $In_2O_3$ sample can be obtained by annealing the $In(OH)_3$ precursor at 500 $^oC$. Clearly the $In_2O_3$ product inherits the morphology of its precursor, as shown in Fig. 3(a). The detailed structure characteristics of them have been described previously. Composition of the as-prepared flower-like $In_2O_3$ hierarchical nanostructures is shown in Fig. 3(b). It is revealed that the sample is composed of In and O elements. Moreover, no impurity was detected, indicating a high purity of the as-prepared products. Fig. 3(c) shows the representative TEM image of a single flower-like $In_2O_3$ nanostructure. It can be seen that the flower-like nanostructure with the diameter of 1.5-2 μm, which is built of a lot of nanoplates. Fig. 3(d) shows that nanoplates of flower-like nanostructures possess a porous structure with a pore-size distribution ranging form 10 to 20 nm. The HRTEM image of a nanoplate at the edge of the flower-like $In_2O_3$ nanostructure is depicted in Fig. 3(e). The observed lattice perpendicular to the nanoplates length is about 0.274 nm, in agreement with the (110) plane of hexagonal phase of $In_2O_3$, demonstrating the nanoplates were mainly dominated by the (110) surface.

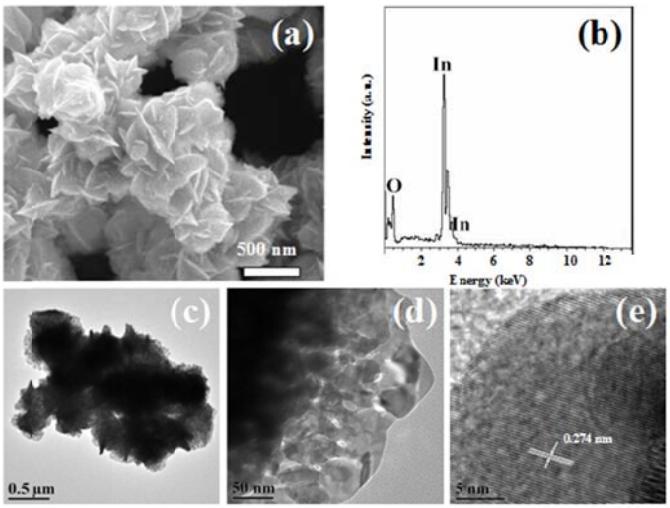


Fig. 3 (a) FESEM image of the $In_2O_3$ sample; (b) EDS pattern of flower-like $In_2O_3$ nanostructure; (c) low and (d) high magnification TEM image of flower-like $In_2O_3$ hierarchical nanostructure; (e) the corresponding HRTEM image with labeled lattice spacing.

To further obtain the information about the pores in the nanoplates, the nitrogen adsorption and desorption measurements were performed at 77 K. Seen from Fig. 4, the prepared $In_2O_3$ products exhibited a hysteresis loop in a high relative pressure range of 0.63-0.94, which was ascribed to a type IV isotherm, indicating the presence of mesopores. The pore size distribution (inserted in Fig. 4) for the desorption branch of the $N_2$ isotherm using the BJH method indicates that flower-like $In_2O_3$ hierarchical nanostructures have an average pore diameter of 18 nm. The result is in good agreement with the TEM image. Since the as-prepared $In_2O_3$ products possess large surface area and mesoporous structure, which are greatly advantageous for gas adsorption-desorption, gas molecular diffusion, and providing more surface sites for oxygen, it is believed that they can be potentially applied in gas sensors with enhanced gas-sensing performance.

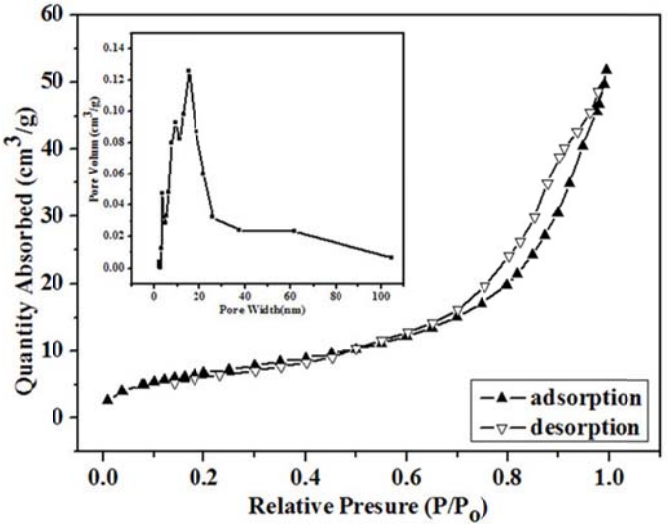


Fig. 4 Typical $N_2$ adsorption- desorption isotherm and BJH pore size distribution plots (inset) of flower-like $In_2O_3$ hierarchical nanostructures.

Based on the above experimental results, we proposed a possible formation mechanism for flower-like $In_2O_3$ hierarchical nanostructures. It was believed that the formation of products could be brought out as the following equations. Firstly, $In^{3+}$ and $[C_6H_5O_7]^{3-}$ are produced after $InCl_3$ and $Na_3C_6H_5O_7{\cdot}2H_2O$ dissolved into the deionized water (Eqs. (3) and (4)). $In^{3+}$ can be easily combined with $[C_6H_5O_7]^{3-}$ via the chelating effect (Eqs. (5)). Urea is an important biological molecule that can decompose and release $OH^-$ in an indirect manner (Eqs. (6) and (7)). Then, $In^{3+}$ will be released and gradually converted into $In(OH)_3$ nuclei via the chemical reaction (Eqs. (8)). Upon hydrothermal treatment, the $In(OH)_3$ nuclei subsequently aggregated to form small particles, followed by their self-assembly into 2D $In(OH)_3$ nanoplates through oriented growth, and then the arrangement of these nanoplates into 3D hierarchical nanostructures,[26-28] as schematically illustrated in Fig. 5. Finally, during the calcination process, the $In(OH)_3$ precursor is converted to $In_2O_3$ (Eqs. (9)). Thermal decomposition of the organic impurity (citrate salt) and the release of $H_2O$ in confined space during the sintered process led to the formation of porous structure.

$$InCl_3 \rightarrow In^{3+} + 3Cl^- \quad (3)$$

$$Na_3C_6O_7H_5 \rightarrow [C_6H_5O_7]^{3-} + 3Na^+ \quad (4)$$

$$In^{3+} + [C_6H_5O_7]^{3-} \rightarrow [C_6H_5O_7]^{3-}\ In^{3+} \quad (5)$$

$$CO(NH_2)_2 + 3H_2O \rightarrow CO_2 + 2NH_3 \cdot H_2O \quad (6)$$

$$NH_3 \cdot H_2O \rightarrow NH_4^+ + OH^- \quad (7)$$

$$[C_6O_7H_5]^{3-}\ In^{3+} + 3OH^- \rightarrow In(OH)_3 + [C_6O_7H_5]^{3-} \quad (8)$$

$$In(OH)_3 \rightarrow In_2O_3 + H_2O \quad (9)$$

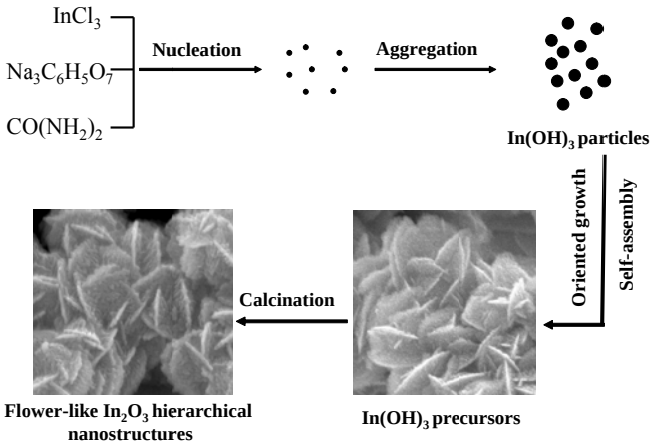


Fig. 5 Schematic illustration of the formation process of flower-like $In_2O_3$ hierarchical nanostructures.

The oriented growth into $In(OH)_3$ nanoplates is possibly induced by the reorientation of the formed $In(OH)_3$ aggregation composed of numerous nuclei, under the present of DMF, in order to minimize the total energy of the reaction system. A similar phenomenon has been reported in the formation of flower-shaped $SnO_2$ nanostructures.[29] Previous reports suggested that the solvent composition has a significant impact on the products morphology.[30, 31] To reveal the influence of DMF during the growth process of flower-like hierarchical nanostructures, the study of morphology evolution of $In(OH)_3$ precursor with different reaction conditions was investigated by changing the $H_2O$-DMF volume ratios, while temperature and reaction time were kept at 170 °C and 14 h, respectively. As shown in Fig. 6(a) and (b), unconsolidated spheres and particles were observed with the $H_2O$-DMF volume ratio of 30:0 and 20:10. When the products were prepared at a volume ratio of 15:15, considerable flower-like hierarchical nanostructures were obtained (Fig. 6(c)). As the sample prepared at volume ratio of 10:20, FESEM image (Fig. 6(d)) showed that $In(OH)_3$ precursor transformed into the sphere-like architecture with diameters of 1 μm, only few plates were detected at the edge of the spheres. When the $H_2O$-DMF volume ratio was 0:30, no product was observed due to the absence of water (Eqs. (6)). FESEM images under different solvent ratios indicated that the solvent composition had a significant influence on the morphologies. And the detailed mechanism for the formation of flower-like $In_2O_3$ hierarchical nanostructures is still under investigation by our group.

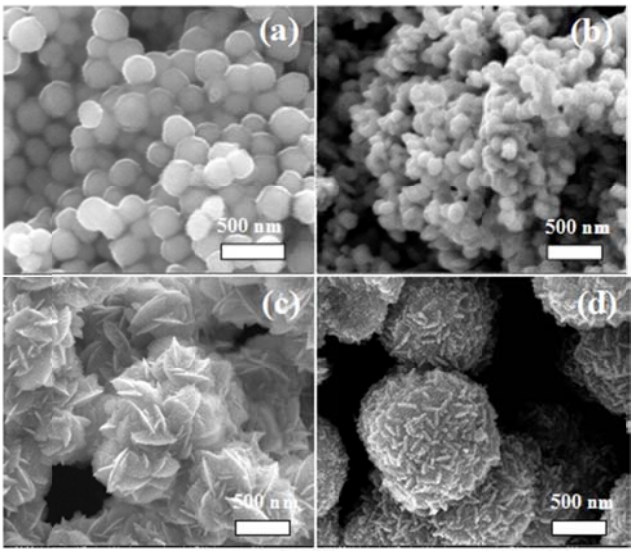


Fig. 6 FESEM images of $In(OH)_3$ precursors prepared with different $H_2O$-DMF volume ratio of (a) 30:0; (b) 20:10; (c) 15:15 and (d) 10:20.

## Gas-sensing properties

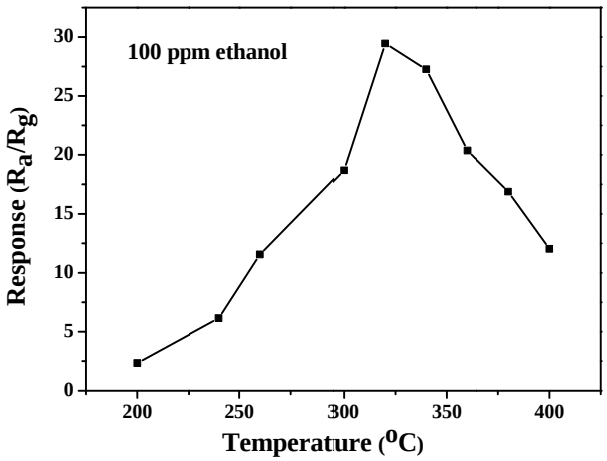


Fig. 7 Response *vs.* operating temperature of flower-like $In_2O_3$ hierarchical nanostructures exposing 100 ppm ethanol.

In general, the response of semiconducting metal oxide gas sensors was dependent on the operating temperature.[32] Therefore, to find the optimum detection temperature, the responses of flower-like $In_2O_3$ hierarchical nanostructures to 100 ppm ethanol were tested as a function of operating temperature from 200 to 400 °C. As shown in Fig. 7, the response was strongly dependent on the operating temperature. As the working temperature increases, a higher response is obtained because of the activation of adsorbed molecular oxygen and lattice oxygen to form active $O^{2-}$ and $O^-$. This phenomenon continues up to a certain optimum temperature, beyond which exothermic gas adsorption becomes difficult and gas molecules begin to desorption in large quantities, leading to a drop in sensor response. Thus, the optimum temperature is a balance point between two conflicting mechanisms.[33, 34] It can be seen that the sensor had an optimum operating temperature of 320 °C, at which the sensor exhibited the highest response of 28 to ethanol gas. As a consequence, we choose 320°C as the optimum operating

temperature to proceed with subsequent investigation in our experiment.

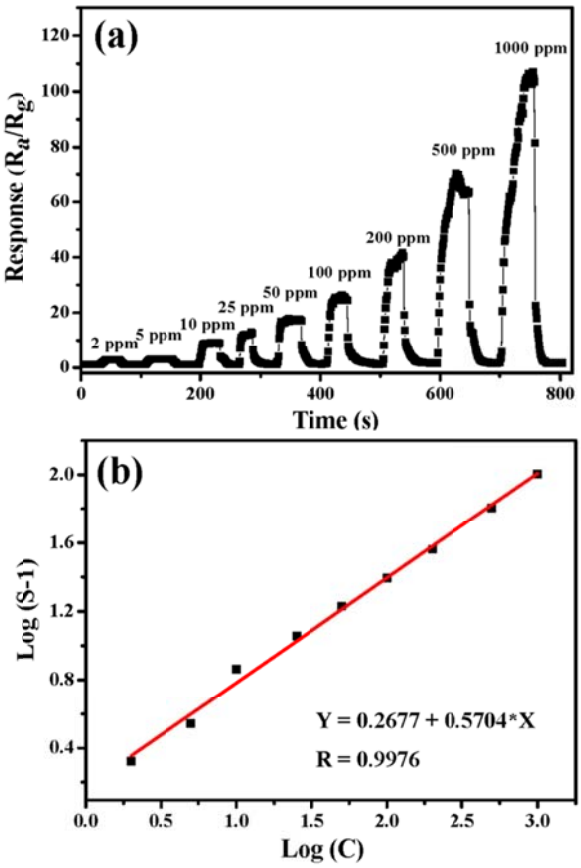


Fig. 8 (a) Typical response curves and variation of the response of flower-like $In_2O_3$ hierarchical nanostructures exposed to different concentration of ethanol ranging from 2 to 1000 ppm and measured at 320 °C; (b) the corresponding log (S-1) *vs*. log (C).

Fig. 8(a) shows the typical response of gas sensors based on flower-like $In_2O_3$ hierarchical nanostructures to 2-1000 ppm ethanol at 320 °C. For the gas sensing mechanism of as-prepared flower-like $In_2O_3$ hierarchical nanostructures, it should belong to the surface-controlled type, which may be explained by the change in resistance of the sensor upon exposure to different gas atmospheres. When the sensors were exposed to air, $O_2$ adsorb on the surface and create chemisorbed oxygen species (such as $O_2^-$, $O^-$ and $O^{2-}$) by capturing electrons from the conductance band through Eqs. (10), resulting in a high resistance state of the $In_2O_3$ samples:

$$O_2\ (gas) \rightarrow O_2\ (ads) \quad (10)$$

$$O_2\ (ads) + e^- \rightarrow O_2^-\ (ads) \quad (11)$$

$$O_2^-\ (ads) + e^- \rightarrow 2\ O^-\ (ads) \quad (12)$$

$$O^-\ (ads) + e^- \rightarrow O^{2-}\ (ads) \quad (13)$$

When the sensors exposed to ethanol vapor at higher temperature, ethanol reacts with the adsorbed oxygen ions reducing their concentration and thereby increasing the semiconductor conductivity. The possible reactions took place on the surface of indium oxide as follows:[35, 36]

$$CH_3CH_2OH + 3O^{2-}_{ads} \rightarrow 2CO_2 + 3H_2O + 6e^- \quad (14)$$

When exposed to air again, the $In_2O_3$ sensors recover to the initial electronic structure. With increasing concentration of ethanol, the sensor response greatly increased. The response can be empirically represented as $S = a[C]^b + 1$, where $a$ and $b$ are the constants and $S$ is the gas response, $C$ is the concentration of the test gas. Generally, the exponent $b$ has an ideal value of either 0.5 or 1. Fig. 8(b) shows a chart of logarithm of the response of the sensor ($S$-1) versus the logarithm of ethanol concentration ($C$). It can be seen that the response of the sensor based on flower-like $In_2O_3$ hierarchical nanostructures has a good linear relationship with the ethanol concentration (2-1000 ppm range) in logarithmic forms, and the value of b towards ethanol was about 0.5704, which was in good agreement with the theory of power laws for semiconductor sensors.[37, 38] The results highlighted the potential applications of the flower-like $In_2O_3$ hierarchical nanostructures in monitoring ethanol gas.

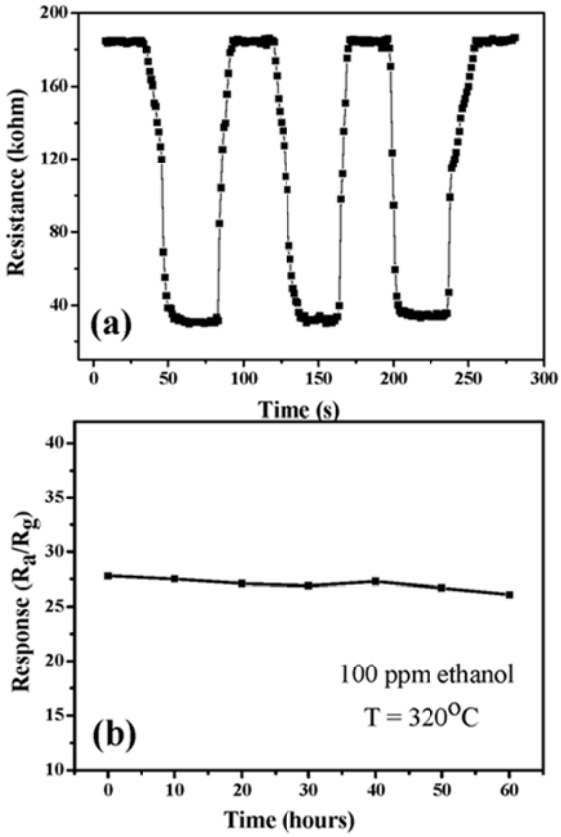


Fig. 9 (a) Reproducibility (3 cycles) and (b) stability of flower-like $In_2O_3$ hierarchical nanostructures sensor on successive exposure to 100 ppm ethanol at 320 °C.

It is evident that the response curves of the sensor increases sharply with increasing concentration of ethanol and then returns to the baseline quickly with the ethanol exhausted out in the closed testing chamber, indicating their quick and reversible response and recovery time. For 100 ppm ethanol gas, 18 s and 9 s are the response and recovery time for flower-like $In_2O_3$ hierarchical nanostructures, respectively. In addition, the flower-like $In_2O_3$ hierarchical nanostructures based sensor exhibits excellent reproducibility as

shown in Fig. 9(a). The sensor maintained its initial response amplitude without a clear decrease upon three successive sensing tests for 100 ppm ethanol. Furthermore, the stability of the sensor was also determined at optimal operating temperature for 60 hours. Clearly, as shown in Fig. 9(b), the senor has nearly constant response to 100 ppm ethanol, which confirmed the high stability of the sensor based on flower-like $In_2O_3$ hierarchical nanostructures.

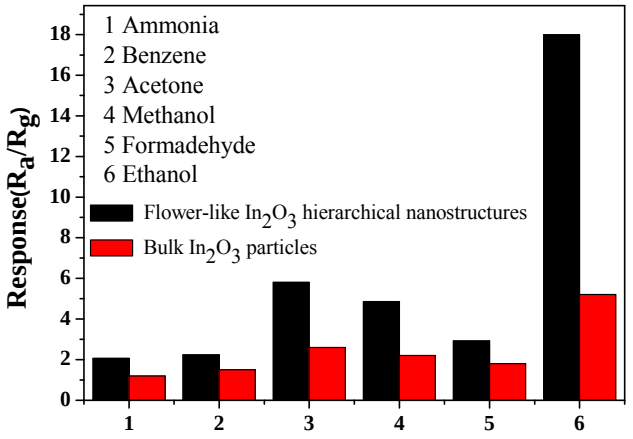


Fig. 10 Responses of flower-like $In_2O_3$ hierarchical nanostructures and bulk particles upon exposure to six kinds of target gases (50 ppm) at a working temperature of 320 °C

A comparative gas sensing study between the as-prepared products and commercial bulk $In_2O_3$ particles prepared by precipitation method was performed to demonstrate the superior ethanol-sensing properties of flower-like $In_2O_3$ hierarchical nanostructures. We have measured the response of flower-like $In_2O_3$ hierarchical nanostructures and bulk $In_2O_3$ particles to six kinds of volatile vapors with a concentration of 50 ppm, such as ammonia, benzene, acetone, methanol, formaldehyde and ethanol at the working temperature of 320 °C (Fig. 10). As expected, the sensor based on flower-like $In_2O_3$ hierarchical nanostructures exhibited enhanced responses for each gas compared with that based on bulk $In_2O_3$ particles. Furthermore, the response of sensor based on flower-like $In_2O_3$ hierarchical nanostructures to ethanol was apparently higher than that to other gases, which seems to depend on the interaction discrepancy between the sensing layer and different testing gas. Furthermore, the response performances of some typical $In_2O_3$-based ethanol gas sensors were listed in Table 1. It should be pointed out that flower-like $In_2O_3$ hierarchical nanostructures in present study possess superior performance when compared with other nanostructured $In_2O_3$ sensors reported in previous works. Consequently, it was concluded that the sensor based on the as-prepared flower-like $In_2O_3$ hierarchical nanostructures showed superior gas sensing performance towards ethanol and it maybe have potential applications in the detection of ethanol vapors.

**Table 1 Gas-sensing properties of various $In_2O_3$ nanostructures to 100 ppm ethanol in the literatures and present study**.

| Sensing $In_2O_3$ nanostructures | Operating temperature (°C) | Sensor response | Response/recovery times (s) | Detection limit (ppm) | Ref |
|---|---|---|---|---|---|
| Flower-like $In_2O_3$ nanostructures | 320 | 27.6 | 18 / 9 | 2 | This work |
| $In_2O_3$:Er hollow spheres | 215 | 40.3 | 10 / 23 | 7 | 39 |
| Nanoporous $In_2O_3$ hollow spheres | 400 | 137.2 | 2 / 830 | 20 | 40 |
| $In_2O_3$ nanospheres | 275 | ~21 | 16 / 24 | 20 | 23 |
| Co-doped $In_2O_3$ nanowires | 300 | ~17 | 2 / 3 | 5 | 41 |
| $In_2O_3$ porous nanoparticles | 200 | ~4 | 6 / 15 | 100 | 42 |
| Mesoporous $In_2O_3$ | 220 | 27.9 | 74 / 119 | 0.05 | 43 |
| Au-loaded $In_2O_3$ nanofibers | 140 | 6.5 | 12 / 24 | 10 | 44 |
| $In_2O_3$ microspheres | 200 | 1.8 | 27 / 24 | 100 | 45 |

## Conclusions

In summary, a simple one-step solution route combined with a subsequent calcining process was reported for the formation of flower-like $In_2O_3$ hierarchical nanostructures, which were composed of many 2-D nanoplates with high porosity. The structure and morphology of $In_2O_3$ samples were investigated in detail, and a possible growth mechanism was supposed from the viewpoint of nucleation and self-assembly of building blocks. Moreover, the gas sensing tests exhibited that flower-like $In_2O_3$ hierarchical nanostructures showed superior gas sensing performance towards ethanol. The results suggest that the as-prepared flower-like $In_2O_3$ hierarchical nanostructures are promising candidates for good performance ethanol sensor.

## Acknowledgements

This work was financially supported by National Natural Science Foundation of China (No. 61102006), Natural Science Foundation of Shandong Province, China (No. ZR2010EQ009).

## Notes and references

*School of Material Science and Engineering, Shandong Provincial Key Laboratory of Preparation and Measurement of Building Materials, University of Jinan, Jinan 250022, China*

** Corresponding author. Tel.: +86 531 82765473; fax: +86 531 87974453*

*E-mail: mse_songp@ujn.edu.cn (P. Song), mse_wangq@ujn.edu.cn (Q. Wang)*

1 G. Neri, A. Bonavita, G. Micali, N. Donato, F.A. Deorsola, P. Mossino, I. Amato and B. De Benedetti, *Sens. Actuators, B*, 2006, **117**, 196−204.
2 P. Ivanov, E. Llobet, X. Vilanova, J. Brezmes, J. Hubalek and X. Correig, *Sens. Actuators, B*, 2004, **99**, 201−206.
3 L. Li, M. M. Liu, S. J. He and W. Chen, *Anal. Chem*., 2014, **86**, 7996−8002.
4 P. P. Jin, X. X. Zou, L. J. Zhou, J. Zhao, H. Chen, Y. Tian and G. D. Li, *Sens. Actuators, B*, 2014, **104**, 142-148.
5 J. Xie, H. Wang and M. Duan, *Sens. Actuators, B*, 2014, **203**, 239-244.
6 X. F. Chu, S. M. Zhou, W. B. Zhang and H. F. Shui, *Mater. Sci. Eng., B*, 2009, **164**, 65-69.
7 S. B. Upadhyay, R. K. Mishra and P. P. Sahay, *Sens. Actuators, B*, 2014, **193**, 19-27.
8 P. Sowti Khiabani, A. Hosseinmardi, E. Marzbanrad, S. Ghashghaiea, C. Zamanic, M. Keyanpour-Radd and B. Raissi, *Sens. Actuators, B*, 2012,**162**, 102-107.
9 P. Sowti Khiabani, E. Marzbanrad, C. Zamani, R. Riahifar and B. Raissi, *Sens. Actuators, B*, 2012, **166-167**, 128-134.
10 T. Wagner, T. Sauerwald, C.-D. Kohl, T. Waitz, C. Weidmann and M. Tiemann, *Thin Solid Films*, 2009, **517**, 6170-6175.
11 P. Y. Song and W. D. Zhang, *Mater. Res. Bull.*, 2014, **53**, 177-184.
12 A. Ayeshamariam, M. Bououdina and C. Sanjeeviraja, *Mater. Sci. Semicond. Process.*, 2013, **16**, 686-695.
13 Z. L. Zhan, J. W. Lu, W. H. Song, D. G. Jiang and J. Q. Xu, *Mater. Res. Bull.*, 2007, 42, 228-235.
14 M. I. Ivanovskaya, D. A. Kotsikaua, A. Taurinob and P. Siciliano, *Sens. Actuators, B*, 2007, **124**, 133-142.
15 H. Ko, S. Park, S. An and C. Lee, *Curr. Appl. Phys.*, 2013, **13**, 919-924.
16 K. Inyawilert, A. Wisitsora-at, A. Tuantranont, P. Singjai, S. Phanichphant, C. Liewhiran, *Sens. Actuators, B*, 2014, **192**, 745-754.
17 C. W. Lai, J. Y. Dai, X. Y. Zhang, H. L. W. Chan, Y. M. Xu, Q. Li, H. C. Ong, *J. Cryst. Growth*, 2005, **282**, 383-388.
18 D. L. Shao, L. Q. Qin, S. Sawyer, *Appl. Surf. Sci.*, 2012, **261**, 123-127.
19. Q. Qi, P. P. Wang, J. Zhao, L. L. Feng, L. J. Zhou, R. F. Xuan, Y. P. Liu, G. D. Li, *Sens. Actuators, B*, 2014, **194**, 440-446.
20 A. Vomiero, S. Bianchi, E. Comini, G. Faglia, M. Ferroni, N. Poli, G. Sberveglieri, *Thin Solid Films*, 2007, **515**, 8356-8359.
21 W. Zeng, H. Zhang, Y. Q. Lia, W. G. Chen, Z. C. Wang, *Mater. Res. Bull.*, 2014, **57**, 91-96.
22 P. Sun, W. Zhao, Y. Cao, Y. Guan, Y.F. Sun, G.Y. Lu, *CrystEngComm*, 2011, **13**, 3718-3724.
23 P. Song, D. Han, H. H. Zhang, J. Li, Z. X. Yang, Q. Wang, *Sens. Actuators, B*, 2014, **196**, 434-439.
24 N. F. Hamedani, A. R. Mahjoub, A. A. khodadadi, Y. Mortazavi, *Sens. Actuators, B*, 2012, **169**, 67-73.
25 J.R. Huang, K. Yua, C.P. Gu, M.H. Zhai, Y.Z. Wu, M. Yang, J.H. Liu, *Sens. Actuators, B*, 2010, **147**, 467-474.
26 J.Y. Liu, T. Luo, F.L. Meng, K. Qian, Y.T. Wan, J.H. Liu, *J. Phys. Chem. C*, 2010, **114**, 4887-4894.
27 J.T. Zai, J. Zhu, R.R. Qi, X.F. Qian, *J. Mater. Chem. A*, 2013, **1**, 735-745.
28 C.Q. Wang, D.R. Chen, X.L. Jiao, *J. Phys. Chem. C*, 2009, **113**, 7714-7718.
29 W. L. Jiao and L. Zhang, *Particuology*, 20130, **11**, 743-747.
30 T. Yan, X. Wang, J. Long, H. Lin, R. Yuan, W. Dai, Z. Li, X. Fu, *New J. Chem*., 2008, **32**, 1843-1846.
31 B.L. Tao, Y. Zhang, D.Z. Han, Y.P. Li, Z.F. Yan, *J. Mater. Chem. A*, 2014, **2**, 5455-5461.
32 Z. Lou, L.L. Wang, T. Fei, T. Zhang, *New J. Chem*., 2012, **36**, 1003-1007.
33 L.J. Bie, X.N. Yan, J. Yin, Y.Q. Duan, Z.H. Yuan, *Sens. Actuators B*, 2007, **126**, 604-608.
34 P. Sun, X. Zhou, C. Wang, K. Shimanoe, G. Lu, N Yamazoe, *J. Mater. Chem. A*, 2014, **2**, 1302-1308.
35 J.Q. Xu, J.J. Han, Y. Zhang, Y.A. Sun, B. Xie, *Sensor. Actuat. B*, 2008, **132**, 334-339.
36 H. Men, P. Gao, B.B. Zhou, Y.J. Chen, C.L. Zhu, G. Xiao, L.Q. Wang, M.L. Zhang, *Chem. Commun*., 2010, **46**, 7581-7583.
37 N. Yamazoe, K. Shimanoe, *Sensor. Actuat. B*, 2008, **128**, 566-573.
38 X.J. Liu, Z. Chang, L. Luo, X.D. Lei, J.F. Liu, X.M. Sun, J. Mater. Chem., 2012, **22**, 7232-7238.
39 T. Zhang, F.B. Gu, D.M. Han, Z.H. Wang, G.S. Guo, *Sens. Actuators*, B, 2013, **177**, 1180-1188.
40 S.J. Kim, I.S. Hwang, J.K. Choi, Y.C. Kang, J.H. Lee, *Sens. Actuators*, B, 2011, **155**, 512-518.
41 Z. Li, Y. Dzenis, *Talanta*, 2011, **85**, 82-85.
42 L. Wang, F. Tang, K. Ozawa, Z.G. Chen, A. Mukherj, Y. Zhu, J. Zou, H.M. Cheng, G.Q. Lu, *Angew. Chem., Int. Ed.*, 2009, **48**, 7048-7051.
43 X.H. Sun, H.R. Hao, H.M. Ji, X.L. Li, S. Cai, C.M. Zheng, *ACS Appl. Mater. Interfaces*, 2014, **6**, 401-409.
44 X.J. Xu, H.T. Fan, Y.T. Liu, L.J. Wang, T. Zhang, K. *Sensor. Actuat. B*, 2011, **160**, 713-719.
45 X.Q. Wang, M.F. Zhang, J.Y. Liu, T. Luo, Y.T. Qian, *Sensor. Actuat. B*, 2009, **137**, 103-110.